International Journal of Solids and Structures 45 (2008) 5716–5729

Contents lists available at ScienceDirect

International Journal of Solids and Structures

journal homepage: www.elsevier.com/locate/ijsolstr

Multiple scattering of electro-elastic waves from a buried cavity in a functionally graded piezoelectric material layer

Xue-Qian Fang *

Department of Engineering Mechanics, Shijiazhuang Railway Institute, Bei erhuandong Road, Shijiazhuang, Hebei 050043, PR China

ARTICLE INFO

Article history:
Received 19 March 2008
Received in revised form 9 May 2008
Available online 26 June 2008

Keywords:
Functionally graded piezoelectric material layer
Multiple scattering of electro-elastic waves
Dynamic stress concentration factor
Circular cavity
Image method

ABSTRACT

This paper presents a theoretical method to investigate the multiple scattering of electro-elastic waves and the dynamic stress around a buried cavity in a functionally graded piezoelectric material layer bonded to a homogeneous piezoelectric material. The analytical solutions of wave fields are expressed by employing wave function expansion method, and the expanded mode coefficients are determined by satisfying the boundary conditions around the cavity. The image method is used to satisfy the mechanical and electrically short conditions at the free surface of the structure. According to the analytical expression of this problem, the numerical solutions of the dynamic stress concentration factor around the cavity are presented. The effects of the piezoelectric property, the position of the cavity in the layer, the incident wave number and the material properties on the dynamic stress around the cavity are analyzed. Analyses show that the piezoelectric property has great effect on the dynamic stress in the region of higher frequencies, and the effect increases with the decrease of the thickness of FGPM layer. If the material properties of the homogeneous piezoelectric material are greater than those at the surface of the structure, the dynamic stress resulting from the piezoelectric property is greater. The effect material properties at the two boundaries of FGPM layer on the distribution of dynamic stress around the cavity is also examined.

1. Introduction

Functionally graded piezoelectric materials (FGPMs) are the new generation of composites and important area of materials science research. In recent years, FGPMs are widely applied in smart materials and structures, so the theoretical investigation on FGPMs has received considerable attention in the literatures. The study of elastic wave propagation through FGPMs has many important applications. Through analysis, we can predict the response of composite materials to various types of loading, and obtain the high strength and toughness of materials. The problem is also a theoretical background of the non-destructive analysis of FGPM microstructures by using ultrasonic technique.

During the serving of composite structures, many failures induced by various loading have been found in these materials. The discontinuities, such as holes, cracks and inclusions in composite structures, are the major reason for these failures. If the discontinuities exist in composite structures, it is definitely vital to determine them and analyze their effects. With the advent of FGPMs, the fracture mechanics under various loading conditions in piezoelectric materials has received much attention in recent years. In the past decade, considerable amounts of analytical, numerical and experimental work about the stress in piezoelectric materials have been done to improve the reliability of structures.

* Tel.: +86 451 86410268; fax: +86 451 89264194.
E-mail addresses: fangxueqian@163.com, fangxueqian@yahoo.com.cn

0020-7683/$ - see front matter © 2008 Elsevier Ltd. All rights reserved.
doi:10.1016/j.ijsolstr.2008.06.014

Up to present time, analyses about the stress problem in FGPMs mainly focus on the behavior under the static loading. Soh et al. (2000) analyzed the behavior of a bi-piezoelectric ceramic layer with a central interfacial crack subjected to anti-plane shear and in-plane electric loading. Using integral transform method, Wang and Noda (2001) discussed the fracture behavior of a cracked smart actuator made of piezoelectric materials with functionally grade material properties. By means of singular integral equation technique, Wang (2003) investigated the mode III crack problem in FGPMs, and both a single crack and a series of collinear cracks were considered. Li and Weng (2002) studied the problem of a finite crack in a strip of FGPMs under an anti-plane mechanical loading and in-plane electric loading. The non-local theory was also applied to obtain the behavior of two collinear cracks in FGPMs under anti-plane shear loading for permeable electric boundary conditions (Zhou and Wu, 2006). By making using of the Gauss–Chebyshev integration technique, Chue and Ou (2005) investigated the singular electromechanical field near the crack tips of an internal crack in FGPMs.

Due to the increasing demand of an understanding of dynamic processes in piezoelectric composites, it is highly desirable to study the stress in FGPMs in a fully dynamic framework. However, considering the complexity of wave scattering resulting from the non-homogeneous property of FGPMs and the complexity of multiple scattering from the scatterer and the boundary, relatively little work has been done regarding on the wave propagation in FGPMs. Recently, Chen et al. (2003) have considered the electromechanical impact response of FGPMs with a crack using integral transform technique. Ma et al. (2004) have investigated the stress and electric displacement intensity factors of two collinear cracks subjected to anti-plane shear waves in FGPMs. Most recently, Fang et al. (2007) studied the dynamic stress from a circular cavity buried in a semi-infinite functionally graded piezoelectric material, and both the displacement field and the piezoelectric field were considered. To the author's knowledge, the multiple scattering of electro-elastic waves and dynamic stress around a cavity in a functionally graded piezoelectric material layer are still unavailable in the literatures.

The objective of this paper is to investigate the analytical solutions of the electro-elastic field and dynamic stress around a cavity embedded in a functionally graded piezoelectric material layer bonded to a homogeneous piezoelectric material. The incidence of anti-plane shear waves at the surface of the structure is applied, and both the displacement field and piezoelectric field in functionally graded piezoelectric materials are presented. The mechanical and electrically short conditions at the free surface are considered, and the image method is used to satisfy the free boundary conditions of the structure. The wave fields and electric potentials are expanded by using wave function expansion method (Pao and Mow, 1973). The expanded mode coefficients are determined by satisfying the boundary conditions around the cavity. Addition theorem for Bessel functions is used to accomplish the translation between different coordinate systems. The analytical solution of the dynamic stress concentration factor around the cavity is presented, and the numerical solutions are graphically illustrated. The effects of the piezoelectric property, the incident wave number and the position of the cavity in the FGPM layer on the dynamic stress concentration factors around the cavity are also analyzed.

2. Wave motion equations in FGPMs and their solutions

Consider a FGPM layer bonded to a homogeneous piezoelectric material, as depicted in Fig. 1. The mechanical and electrically short conditions at the free surface are considered. $c_{44}^1, e_{15}^1, \varepsilon_{11}^1, \rho^1$ are the elastic stiffness, piezoelectric constant, dielectric constant and density of materials at the surface of FGPM layer, and $c_{44}^2, e_{15}^2, \varepsilon_{11}^2, \rho^2$ those of the homogeneous piezoelectric material. The material properties in the FGPM layer vary smoothly along the x-direction. Let a circular cavity lie in the functionally graded piezoelectric material layer. The distance between the center of the cavity and the upper edge of the layer is h_1, and that between the center of the cavity and the lower edge of the FGPM layer is h_2.

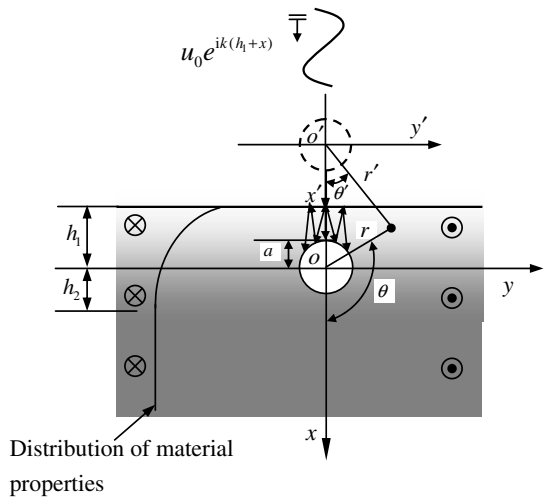

Fig. 1. Schematic of the buried cavity and the incident elastic waves in a functionally graded piezoelectric material layer.

All materials exhibit transversely isotropic behavior and are polarized in the z-direction. Let an anti-plane shear wave with frequency ω hit the surface of the FGPM layer in the positive x-direction. In this case, the mechanically and electrically coupled constitutive equations can be written as

$$\sigma_{zx} = c_{44}(x)\frac{\partial u}{\partial x} + e_{15}(x)\frac{\partial \phi}{\partial x}, \quad \sigma_{zy} = c_{44}(x)\frac{\partial u}{\partial y} + e_{15}(x)\frac{\partial \phi}{\partial y}, \tag{1}$$

$$D_x = e_{15}(x)\frac{\partial u}{\partial x} - \varepsilon_{11}(x)\frac{\partial \phi}{\partial x}, \quad D_y = e_{15}(x)\frac{\partial u}{\partial y} - \varepsilon_{11}(x)\frac{\partial \phi}{\partial y}, \tag{2}$$

where σ_{zj}, u, D_j and $\phi(j = x,y)$ are the shear stress, anti-plane displacement, in-plane electric displacement and electric potential, respectively; $c_{44}(x)$ is the elastic stiffness of graded materials measured in a constant electric field, $\varepsilon_{11}(x)$ is the dielectric constant of graded materials measured in constant strain and $e_{15}(x)$ is the piezoelectric constant of graded materials.

The anti-plane governing equation and Maxwell's equation in FGPMs are described as

$$\frac{\partial \sigma_{zx}}{\partial x} + \frac{\partial \sigma_{zy}}{\partial y} = \rho(x)\frac{\partial^2 u}{\partial t^2}, \tag{3}$$

$$\frac{\partial D_x}{\partial x} + \frac{\partial D_y}{\partial y} = 0, \tag{4}$$

Substituting Eqs. (1) and (2) into Eqs. (3) and (4), the following equations can be obtained:

$$\frac{\partial c_{44}(x)}{\partial x}\frac{\partial u}{\partial x} + c_{44}(x)\frac{\partial^2 u}{\partial x^2} + \frac{\partial e_{15}(x)}{\partial x}\frac{\partial \phi}{\partial x} + e_{15}(x)\frac{\partial^2 \phi}{\partial x^2} + c_{44}(x)\frac{\partial^2 u}{\partial y^2} + e_{15}(x)\frac{\partial^2 \phi}{\partial y^2} = \rho(x)\frac{\partial^2 u}{\partial t^2}, \tag{5}$$

$$\frac{\partial e_{15}(x)}{\partial x}\frac{\partial u}{\partial x} + e_{15}(x)\frac{\partial^2 u}{\partial x^2} - \frac{\partial \varepsilon_{11}(x)}{\partial x}\frac{\partial \phi}{\partial x} - \varepsilon_{11}(x)\frac{\partial^2 \phi}{\partial x^2} + e_{15}(x)\frac{\partial^2 u}{\partial y^2} - \varepsilon_{11}(x)\frac{\partial^2 \phi}{\partial y^2} = 0. \tag{6}$$

For convenience, it is assumed that all material properties vary continuously and have the same exponential function distribution along the x-direction in the layer, i.e.

$$c_{44}(x) = c_{44}^0 \exp(2\beta x), \quad e_{15}(x) = e_{15}^0 \exp(2\beta x), \quad \varepsilon_{11}(x) = \varepsilon_{11}^0 \exp(2\beta x), \quad \rho(x) = \rho^0 \exp(2\beta x), \tag{7}$$

According to the continuous condition of the material properties in the layer and at the position of $x = h_2$, the constants $\beta, c_{44}^0, e_{15}^0, \varepsilon_{11}^0$ and ρ^0 can be calculated as

$$\beta = \frac{1}{2(h_1 + h_2)} \ln\left(\frac{c_{44}^2}{c_{44}^1}\right), \tag{8}$$

$$c_{44}^0 = c_{44}^1 \exp(2\beta h_1), \quad e_{15}^0 = e_{15}^1 \exp(2\beta h_1), \quad \varepsilon_{11}^0 = \varepsilon_{11}^1 \exp(2\beta h_1), \quad \rho^0 = \rho^1 \exp(2\beta h_1). \tag{9}$$

In the above formulations, it is assumed that the ratio c_{44}^2/c_{44}^1 is equal to e_{15}^2/e_{15}^1, $\varepsilon_{11}^2/\varepsilon_{11}^1$, and ρ^2/ρ^1. Though the variations are unrealistic, it would allow us to comprehend the effect of material properties of FGPMs on the dynamic stress around the cavity and can provide references for the non-destruction detection in FGPMs.

Substituting Eq. (7) into Eqs. (5) and (6), the following equations are obtained:

$$2\beta c_{44}^0 \frac{\partial u}{\partial x} + c_{44}^0 \nabla^2 u + 2\beta e_{15}^0 \frac{\partial \phi}{\partial x} + e_{15}^0 \nabla^2 \phi = 2\beta \rho^0 \frac{\partial^2 u}{\partial t^2}, \tag{10}$$

$$2\beta e_{15}^0 \frac{\partial u}{\partial x} + e_{15}^0 \nabla^2 u = 2\beta \varepsilon_{11}^0 \frac{\partial \phi}{\partial x} + \varepsilon_{11}^0 \nabla^2 \phi. \tag{11}$$

Here, $\nabla^2 = \partial^2/\partial x^2 + \partial^2/\partial\, y^2$ is the two-dimensional Laplace operator in the variables x and y.

Assume that another electro-elastic field ψ is expressed as

$$\psi = \phi - \lambda_1 u, \tag{12}$$

where $\lambda_1 = e_{15}^0/\varepsilon_{11}^0$.

From Eqs. (10) and (11), the following equations can be obtained:

$$\nabla^2 u + 2\beta \frac{\partial u}{\partial x} = \frac{1}{c_{SH}^2}\frac{\partial^2 u}{\partial t^2}, \tag{13}$$

$$2\beta \frac{\partial \psi}{\partial x} + \nabla^2 \psi = 0, \tag{14}$$

where $c_{SH} = \sqrt{\mu^e/\rho^0}$ with $\mu^e = c_{44}^0 + [(e_{15}^0)^2/\varepsilon_{11}^0]$ being the wave speed of electro-elastic waves.

The steady solution of this problem is investigated. Assuming that $u = u_0 U e^{-i\omega t}$, Eq. (13) can be changed into

$$\nabla^2 U + 2\beta\frac{\partial U}{\partial x} + k^2 U = 0, \tag{15}$$

where ω is the frequency of the incident waves and $k = \omega/c_{SH}$ is the wave number of incident waves.

To solve Eq. (15), the solution can be proposed as

$$U = \exp(-\beta x) w(x, y), \tag{16}$$

where $w(x,y)$ is the function introduced for derivation.

Substituting Eq. (16) into Eq. (15), one can see that the function $w(x,y)$ should satisfy the following equation:

$$\nabla^2 w + \kappa^2 w = 0, \tag{17}$$

Here, $\kappa = \sqrt{(k^2 - \beta^2)}$.

According to Eqs. (15)–(17), one can see that there exist elastic waves with the form of $u = u_0 U e^{-i\omega t} = u_0 \exp(-\beta x) e^{i(\kappa x - \omega t)}$, which denotes the propagating wave with its amplitude of vibration attenuating in the x-direction.

Similarly, the solution of ψ in Eq. (14) has the following form:

$$\psi = \psi_0 \exp(-\beta x) e^{i(i\beta x - \omega t)}. \tag{18}$$

Note that all field quantities have the same time variation $e^{-i\omega t}$, which is suppressed in all subsequent representations for notational convenience.

According to Eqs. (14) and (17), the general solutions of the scattered field of electro-elastic waves resulting from the cavity in FGPMs can be described, using wave function expansion method (Pao and Mow, 1973), as

$$u^s = \exp(-\beta r\cos\theta) \sum_{n=-\infty}^{\infty} a_n H_n^{(1)}(\kappa r) e^{in\theta}, \tag{19}$$

$$\psi^s = \exp(-\beta r\cos\theta) \sum_{n=-\infty}^{\infty} b_n H_n^{(1)}(i\beta r) e^{in\theta}, \tag{20}$$

where (r,θ) is the corresponding cylindrical coordinate system shown in Fig. 1, $H_n^{(1)}(\cdot)$ is the nth Hankel function of the first kind, and a_n and b_n determined by satisfying the boundary conditions are the mode coefficients of the scattered waves. Note that Hankel function $H_n^{(1)}(\cdot)$ denotes the outgoing wave and satisfies the radiation condition at infinity. The solution of the scattered–reflected waves has the same form as that of the scattered waves (Fang et al., 2006).

3. The multiple scattering of electro-elastic waves and the total wave field

Consider the electro-elastic waves propagating along the positive x-direction in the FGPM structure. In the local coordinate system (r,θ) of the real cavity, the incident waves can be expanded as Pao and Mow (1973)

$$u_1^{(i)} = u_0 \exp[-\beta x + h_1(i\kappa - \beta)] e^{i\kappa x} = u_0 \exp[-\beta r\cos\theta + h_1(i\kappa - \beta)] \sum_{n=-\infty}^{\infty} i^n J_n(\kappa r) e^{in\theta}, \tag{21}$$

where u_0 is the amplitude of the incident waves, κ is the wave number of the propagating waves and $J_n(\cdot)$ is the nth Bessel function of the first kind.

Similarly, the incident field $\psi^{(i)}$ is expressed as

$$\psi_1^{(i)} = \lambda_1 u_0 \exp(-\beta x - 2\beta h_1) e^{-\beta x} = \lambda_1 u_0 \exp(-\beta r\cos\theta - 2\beta h_1) \sum_{n=-\infty}^{\infty} i^n J_n(i\beta r) e^{in\theta}. \tag{22}$$

In the local coordinate system (r,θ) of the real cavity, the scattered field can be described as

$$u_1^{(s)} = \exp(-\beta r\cos\theta) \sum_{l=1}^{\infty} \sum_{n=-\infty}^{\infty} A_{n1}^l H_n^{(1)}(\kappa r) e^{in\theta}, \tag{23}$$

$$\psi_1^{(s)} = \lambda_1 \exp(-\beta r\cos\theta) \sum_{l=1}^{\infty} \sum_{n=-\infty}^{\infty} B_{n1}^l H_n^{(1)}(i\beta r) e^{in\theta}. \tag{24}$$

where l denotes the scattering time between the real and image cavities, and A_n^l and B_n^l $(l = 1, 2, \ldots, \infty)$ determined by satisfying the boundary conditions are the mode coefficients of the lth scattering resulting from the real cavity.

When the electro-elastic wave propagates in the FGPM layer, it is scattered by the circular cavity at first. Then, the outgoing scattered wave from the cavity is reflected on the straight surface ($x = -h_1$), and the reflected waves arise. The reflected waves are scattered by the cavity again. This complex phenomenon is shown in Fig. 1.

To satisfy the mechanical and electrically short conditions at the free surface, the image method is applied. The reflected waves at the edge of FGPM layer are described by the scattered waves resulting from the virtual image cavity. The distance between the virtual image cavity and the straight boundary is also h_1. The magnitudes of the incident waves and scattered waves of the real and image cavities are the same, however, the directions of them are opposite. So, the boundary conditions at the free surface can be satisfied.

For the image cavity, the waves propagate in the negative x'-direction and can be expressed as

$$u_2^{(i)} = u_0 \exp[\beta x' + h_1(\mathrm{i}\kappa - \beta)]\mathrm{e}^{-\mathrm{i}\kappa x'} = u_0 \exp[\beta r' \cos\theta + h_1(\mathrm{i}\kappa - \beta)] \sum_{n=-\infty}^{\infty} \mathrm{i}^{-n} J_n(\kappa r')\mathrm{e}^{\mathrm{i}n\theta'}, \tag{25}$$

$$\psi_2^{(i)} = \lambda_1 u_0 \exp(\beta x' - 2\beta h_1)\mathrm{e}^{\beta x'} = \lambda_1 u_0 \exp(\beta r' \cos\theta - 2\beta h_1) \sum_{n=-\infty}^{\infty} \mathrm{i}^{-n} J_n(\mathrm{i}\beta r')\mathrm{e}^{\mathrm{i}n\theta'}. \tag{26}$$

Likewise, in the local coordinate system (r', θ'), the scattered fields resulting from the image cavity can be described as

$$u_2^{(s)} = \exp(\beta r' \cos\theta') \sum_{l=1}^{\infty} \sum_{n=-\infty}^{\infty} A_{n2}^l H_n^{(1)}(\kappa r')\mathrm{e}^{\mathrm{i}n\theta'}, \tag{27}$$

$$\psi_2^{(s)} = \lambda_1 \exp(\beta r' \cos\theta') \sum_{l=1}^{\infty} \sum_{n=-\infty}^{\infty} B_{n2}^l H_n^{(1)}(\mathrm{i}\beta r')\mathrm{e}^{\mathrm{i}n\theta'}, \tag{28}$$

where A_{n2}^l and B_{n2}^l $(l = 1, 2, \ldots, \infty)$ determined by satisfying the boundary conditions are the mode coefficients of the $l$thscattering resulting from the image cavity.

Thus, the total field of elastic waves in the material is taken to be the superposition of the incident field, the scattered field and the reflected field at the surface of materials, namely,

$$u^t = u_1^{(i)} + u_1^{(s)} + u_2^{(s)}. \tag{29}$$

So, the total electric potential in the material is expressed as

$$\phi^t = \lambda_1 u^t + \psi_1^{(i)} + \psi_1^{(s)} + \psi_2^{(s)}. \tag{30}$$

In the cavity, the elastic wave field vanishes and only the electric field exists. The electric potential in the real cavity is the standing wave and is expressed as

$$\phi_1^{\mathrm{I}} = \lambda_1 \sum_{l=1}^{\infty} \sum_{n=-\infty}^{\infty} C_{n1}^l J_n(\mathrm{i}\beta r)\mathrm{e}^{\mathrm{i}n\theta}. \tag{31}$$

Similarly, the electric potential in the image cavity is written as

$$\phi_2^{\mathrm{I}} = \lambda_1 \sum_{l=1}^{\infty} \sum_{n=-\infty}^{\infty} C_{n2}^l J_n(\mathrm{i}\beta r')\mathrm{e}^{\mathrm{i}n\theta'}. \tag{32}$$

To make computation tractable, the expression of elastic fields and electric fields in the local coordinate system (r', θ') can be translated into another local coordinate system (r, θ). According to addition theorem for Bessel functions (Stratton, 1941), the following relation can be derived:

$$H_n^{(1)}(pr')\mathrm{e}^{\mathrm{i}n\theta'} = \sum_{m=-\infty}^{\infty} (-1)^{m-n} H_{m-n}^{(1)}(2ph_1) J_m(pr)\mathrm{e}^{\mathrm{i}m\theta}. \tag{33}$$

Similarly,

$$H_n^{(1)}(pr)\mathrm{e}^{\mathrm{i}n\theta} = \sum_{m=-\infty}^{\infty} H_{m-n}^{(1)}(2ph_1) J_m(pr')\mathrm{e}^{\mathrm{i}m\theta'}. \tag{34}$$

So, the following translation of coordinate systems can be obtained:

$$\exp(\beta r' \cos\theta') \sum_{n=-\infty}^{\infty} H_n^{(1)}(pr')\mathrm{e}^{\mathrm{i}n\theta'} = \exp[\beta(2h_1 + r\cos\theta)] \times \sum_{n=-\infty}^{\infty} \sum_{m=-\infty}^{\infty} (-1)^{m-n} H_{m-n}^{(1)}(2ph_1) J_m(pr)\mathrm{e}^{\mathrm{i}m\theta}, \tag{35}$$

where $r' = \sqrt{r^2 + 4h_1^2 + 4rh_1\cos\theta}$ and $\cos\theta' = ((r')^2 + 4h_1^2 - r^2)/4h_1 r'$.

$$\exp(-\beta r \cos\theta) \sum_{n=-\infty}^{\infty} H_n^{(1)}(pr)\mathrm{e}^{\mathrm{i}n\theta} = \exp[\beta(2h_1 - r'\cos\theta')] \sum_{n=-\infty}^{\infty} \sum_{m=-\infty}^{\infty} H_{m-n}^{(1)}(2ph_1) J_m(pr')\mathrm{e}^{\mathrm{i}m\theta'}, \tag{36}$$

where $r = \sqrt{(r')^2 + 4h_1^2 - 4r'h_1\cos\theta'}$, and $\cos\theta = -(r^2 + 4h_1^2 - (r')^2)/4h_1 r$.

4. Boundary conditions around the cavity

Without loss of generality, the case that the cavity is free of traction is investigated. For the cavity, the boundary conditions around it are that the radial shear stress is equal to zero, and the electric potential and normal electric displacement are continuous. They can be expressed as

$$\sigma_{rz}|_{r=a} = \left.\frac{\partial u^t}{\partial r}\right|_{r=a} + \lambda_2 \left.\frac{\partial \phi^t}{\partial r}\right|_{r=a} = 0, \tag{37}$$

$$D|_{r=a} = e_{15}\left.\frac{\partial u^t}{\partial r}\right|_{r=a} - \varepsilon_{11}\left.\frac{\partial \phi^t}{\partial r}\right|_{r=a} = -\varepsilon_0 \left.\frac{\partial \phi^l}{\partial r}\right|_{r=a}, \quad \lambda_3 \left.\frac{\partial(\psi_1^{(i)} + \psi_1^{(s)} + \psi_2^{(s)})}{\partial r}\right|_{r=a} = \left.\frac{\partial \phi^l}{\partial r}\right|_{r=a}. \tag{38}$$

$$\phi^t|_{r=a} = \phi^l|_{r=a}. \tag{39}$$

Here, $\lambda_2 = e_{15}^0/c_{44}^0$ and $\lambda_3 = \varepsilon_{11}^0/\varepsilon_0$. Note that $\varepsilon_0 = 8.85 \times 10^{-12}$ F/m is the dielectric constant of vacuum.

5. Determination of scattering mode coefficients and dynamic stress concentration factor

Multiple scattering of waves takes place between the real and image cavities. By satisfying the boundary conditions around the cavities, the mode coefficients of electro-elastic waves are determined. Substituting Eqs. (29)–(32) into Eqs. (37)–(39), multiplying by $e^{-is\theta}$ at both sides of Eqs. (37)–(39), and then integrating from $-\pi$ to π, the following recurrence formulae can be obtained.

When $l = 1$, the relations among every mode coefficient of the scattered waves are written as

$$\begin{aligned}
&(1+\lambda_1\lambda_2)A_{s1}^1\{\beta a\cos\theta H_s^{(1)}(\kappa a) - [sH_s^{(1)}(\kappa a) - \kappa a H_{s+1}^{(1)}(\kappa a)]\} \\
&\quad + \lambda_1\lambda_2 B_{s1}^1\{\beta a\cos\theta H_s^{(1)}(\mathrm{i}\beta a) - [sH_s^{(1)}(\mathrm{i}\beta a) - \mathrm{i}\beta a H_{s+1}^{(1)}(\mathrm{i}\beta a)]\} \\
&\quad = -(1+\lambda_1\lambda_2)\mathrm{i}^s \exp[h_1(\mathrm{i}\kappa - \beta)]\{\beta a\cos\theta J_s(\kappa a) - [sJ_s(\kappa a) - \kappa a J_{s+1}(\kappa a)]\} \\
&\quad\quad - \lambda_1\lambda_2 \mathrm{i}^s \exp(-2\beta h_1)\{\beta a\cos\theta J_s(\mathrm{i}\beta a) - [sJ_s(\mathrm{i}\beta a) - \mathrm{i}\beta a J_{s+1}(\mathrm{i}\beta a)]\}.
\end{aligned} \tag{40}$$

$$\begin{aligned}
&(1+\lambda_1\lambda_2)A_{s2}^1\{\beta a\cos\theta' H_s^{(1)}(\kappa a) + [sH_s^{(1)}(\kappa a) - \kappa a H_{s+1}^{(1)}(\kappa a)]\} \\
&\quad + \lambda_1\lambda_2 B_{s2}^1\{\beta a\cos\theta' H_s^{(1)}(\mathrm{i}\beta a) + [sH_s^{(1)}(\mathrm{i}\beta a) - \mathrm{i}\beta a H_{s+1}^{(1)}(\mathrm{i}\beta a)]\} \\
&\quad = -(1+\lambda_1\lambda_2)\mathrm{i}^{-s} \exp[h_1(\mathrm{i}\kappa - \beta)]\{\beta a\cos\theta' J_s(\kappa a) + [sJ_s(\kappa a) - \kappa a J_{s+1}(\kappa a)]\} \\
&\quad\quad - \lambda_1\lambda_2 \mathrm{i}^{-s} \exp(-2\beta h_1)\{\beta a\cos\theta J_s(\mathrm{i}\beta a) + [sJ_s(\mathrm{i}\beta a) - \kappa a J_{s+1}(\mathrm{i}\beta a)]\}.
\end{aligned} \tag{41}$$

$$\begin{aligned}
&\lambda_1\lambda_3 B_{s1}^1\{\beta a\cos\theta H_s^{(1)}(\mathrm{i}\beta a) - [sH_s^{(1)}(\mathrm{i}\beta a) - \mathrm{i}\beta a H_{s+1}^{(1)}(\mathrm{i}\beta a)]\} \\
&\quad - \lambda_1 C_{s1}^1\{\beta a\cos\theta J_s(\mathrm{i}\beta a) - [sJ_s(\mathrm{i}\beta a) - \mathrm{i}\beta a J_{s+1}(\mathrm{i}\beta a)]\} \\
&\quad = -\lambda_1\lambda_3 \mathrm{i}^s \exp(-2\beta h_1)\{\beta a\cos\theta J_s(\mathrm{i}\beta a) - [sJ_s(\mathrm{i}\beta a) - \mathrm{i}\beta a J_{s+1}(\mathrm{i}\beta a)]\}.
\end{aligned} \tag{42}$$

$$\begin{aligned}
&\lambda_1\lambda_3 B_{s2}^1\{\beta a\cos\theta' H_s^{(1)}(\mathrm{i}\beta a) + [sH_s^{(1)}(\mathrm{i}\beta a) - \mathrm{i}\beta a H_{s+1}^{(1)}(\mathrm{i}\beta a)]\} \\
&\quad - \lambda_1 C_{s2}^1\{\beta a\cos\theta' J_s(\mathrm{i}\beta a) + [sJ_s(\mathrm{i}\beta a) - \mathrm{i}\beta a J_{s+1}(\mathrm{i}\beta a)]\} \\
&\quad = -\lambda_1\lambda_3 \mathrm{i}^{-s} \exp(-2\beta h_1)\{\beta a\cos\theta' J_s(\mathrm{i}\beta a) + [sJ_s(\mathrm{i}\beta a) - \mathrm{i}\beta a J_{s+1}(\mathrm{i}\beta a)]\}.
\end{aligned} \tag{43}$$

$$A_{s1}^1 H_s^{(1)}(\kappa a) + B_{s1}^1 H_s^{(1)}(\mathrm{i}\beta a) - C_{s1}^1 J_s(\mathrm{i}\beta a) = -\mathrm{i}^s \exp(-2\beta h_1)[J_s(\kappa a) + J_s(\mathrm{i}\beta a)]. \tag{44}$$

$$A_{s2}^1 H_s^{(1)}(\kappa a) + B_{s2}^1 H_s^{(1)}(\mathrm{i}\beta a) - C_{s2}^1 J_s(\mathrm{i}\beta a) = -\mathrm{i}^{-s} \exp(-2\beta h_1)[J_s(\kappa a) + J_s(\mathrm{i}\beta a)]. \tag{45}$$

When $l = 2,3,\ldots,\infty$, the relations among every mode coefficient of the scattered waves are written as

$$\begin{aligned}
&A_{s1}^l(1+\lambda_1\lambda_2)\exp(-\beta a\cos\theta)\{-\beta a\cos\theta H_s^{(1)}(\kappa a) + [sH_s^{(1)}(\kappa a) - \kappa a H_{s+1}^{(1)}(\kappa a)]\} \\
&\quad + B_{s1}^l\lambda_1\lambda_2\exp(-\beta a\cos\theta)\{-\beta a\cos\theta H_s^{(1)}(\mathrm{i}\beta a) + [sH_s^{(1)}(\mathrm{i}\beta a) - \mathrm{i}\beta a H_{s+1}^{(1)}(\mathrm{i}\beta a)]\} \\
&\quad = -A_{s2}^{l-1}(1+\lambda_1\lambda_2)\exp[\beta(2h_1 + a\cos\theta)]\left\{\beta a\cos\theta \sum_{m=-\infty}^{\infty}(-1)^{s-m}H_{s-m}^{(1)}(2\kappa h_1)J_s(\kappa a)\right. \\
&\quad\quad \left. + \sum_{m=-\infty}^{\infty}(-1)^{s-m}H_{s-m}^{(1)}(2\kappa h_1)[sJ_s(\kappa a) - \kappa a J_{s+1}(\kappa a)]\right\}
\end{aligned}$$

$$
\begin{aligned}
&- \lambda_1\lambda_2 B_{s2}^{l-1}\exp[\beta(2h_1+a\cos\theta)]\Bigg\{\beta a\cos\theta\sum_{m=-\infty}^{\infty}(-1)^{s-m}H_{s-m}^{(1)}(2\mathrm{i}\beta h_1)J_s(\mathrm{i}\beta a)\\
&+\sum_{m=-\infty}^{\infty}(-1)^{s-m}H_{s-m}^{(1)}(2\mathrm{i}\beta h_1)[sJ_s(\mathrm{i}\beta a)-\mathrm{i}\beta a J_{s+1}(\mathrm{i}\beta a)]\Bigg\},\\
&\quad(l=2,3,\ldots,\infty).
\end{aligned}\tag{46}
$$

$$
\begin{aligned}
&(1+\lambda_1\lambda_2)A_{s2}^{l}\exp(\beta a\cos\theta')\{\beta a\cos\theta' H_s^{(1)}(\kappa a)+[sH_s^{(1)}(\kappa a)-\kappa a H_{s+1}^{(1)}(\kappa a)]\}\\
&+\lambda_1\lambda_2 B_{s2}^{l}\exp(\beta a\cos\theta')\{\beta a\cos\theta' H_s^{(1)}(\mathrm{i}\beta a)+[sH_s^{(1)}(\mathrm{i}\beta a)-\mathrm{i}\beta a H_{s+1}^{(1)}(\mathrm{i}\beta a)]\}\\
&=-(1+\lambda_1\lambda_2)A_{s1}^{l-1}\exp[\beta(2h_1-a\cos\theta')]\Bigg\{-\beta a\cos\theta'\sum_{m=-\infty}^{\infty}H_{s-m}^{(1)}(2\kappa h_1)J_s(\kappa a)\\
&+\sum_{m=-\infty}^{\infty}H_{s-m}^{(1)}(2\kappa h_1)[sJ_s(\kappa a)-\kappa a J_{s+1}(\kappa a)]\Bigg\}\\
&-\lambda_1\lambda_2 B_{s1}^{l-1}\exp[\beta(2h_1-a\cos\theta')]\Bigg\{\beta a\cos\theta'\sum_{m=-\infty}^{\infty}H_{s-m}^{(1)}(2\mathrm{i}\beta h_1)J_s(\mathrm{i}\beta a)\\
&+\sum_{m=-\infty}^{\infty}H_{s-m}^{(1)}(2\mathrm{i}\beta h_1)[sJ_s(\mathrm{i}\beta a)-\mathrm{i}\beta a J_{s+1}(\mathrm{i}\beta a)]\Bigg\},\\
&\quad(l=2,3,\ldots,\infty)
\end{aligned}\tag{47}
$$

$$
\begin{aligned}
&\lambda_1\lambda_3 B_{s1}^{l}\exp(-\beta a\cos\theta)\{-\beta a\cos\theta H_s^{(1)}(\mathrm{i}\beta a)+[sH_s^{(1)}(\mathrm{i}\beta a)-\mathrm{i}\beta a H_{s+1}^{(1)}(\mathrm{i}\beta a)]\}\\
&-\lambda_1 C_{s1}^{1}[sJ_s(\mathrm{i}\beta a)-\mathrm{i}\beta a J_{s+1}(\mathrm{i}\beta a)]\\
&=-\lambda_1\lambda_3 B_{s2}^{l-1}\exp[\beta(2h_1+a\cos\theta)]\Bigg\{\beta a\cos\theta\sum_{m=-\infty}^{\infty}(-1)^{s-m}H_{s-m}^{(1)}(2\mathrm{i}\beta h_1)J_s(\mathrm{i}\beta a)\\
&+\sum_{m=-\infty}^{\infty}(-1)^{s-m}H_{s-m}^{(1)}(2\mathrm{i}\beta h_1)[sJ_s(\mathrm{i}\beta a)-\mathrm{i}\beta a J_{s+1}(\mathrm{i}\beta a)]\Bigg\},\\
&\quad(l=2,3,\ldots,\infty).
\end{aligned}\tag{48}
$$

$$
\begin{aligned}
&\lambda_1\lambda_3 B_{s2}^{l}\exp(\beta a\cos\theta')\{\beta a\cos\theta' H_s^{(1)}(\mathrm{i}\beta a)+[sH_s^{(1)}(\mathrm{i}\beta a)-\mathrm{i}\beta a H_{s+1}^{(1)}(\mathrm{i}\beta a)]\}\\
&-\lambda_1 C_{s2}^{1}[sJ_s(\mathrm{i}\beta a)-\mathrm{i}\beta a J_{s+1}(\mathrm{i}\beta a)]\\
&-\lambda_1\lambda_3 B_{s1}^{l-1}\exp[\beta(2h_1-a\cos\theta')]\Bigg\{\beta a\cos\theta'\sum_{m=-\infty}^{\infty}H_{s-m}^{(1)}(2\mathrm{i}\beta h_1)J_n(\mathrm{i}\beta a)\\
&+\sum_{m=-\infty}^{\infty}H_{s-m}^{(1)(2\mathrm{i}\beta h_1)[sJ_s(\mathrm{i}\beta a)-\mathrm{i}\beta a J_{s+1}(\mathrm{i}\beta a)]}\Bigg\},\\
&\quad(l=2,3,\ldots,\infty),
\end{aligned}\tag{49}
$$

$$
\begin{aligned}
&\exp(-\beta a\cos\theta)\{A_{s1}^{l}H_s^{(1)}(\kappa a)+B_{s1}^{l}H_s^{(1)}(\mathrm{i}\beta a)\}-C_{n1}^{l}J_n(\mathrm{i}\beta a)\\
&=-\exp[\beta(2h_1+a\cos\theta)]\\
&\times\Bigg\{A_{s2}^{l-1}\sum_{m=-\infty}^{\infty}(-1)^{s-m}H_{s-m}^{(1)}(2\kappa h_1)J_s(\kappa a)+B_{s2}^{l-1}\sum_{m=-\infty}^{\infty}(-1)^{s-m}H_{s-m}^{(1)}(2\mathrm{i}\beta h_1)J_s(\mathrm{i}\beta a)\Bigg\},\\
&\quad(l=2,3,\ldots,\infty).
\end{aligned}\tag{50}
$$

$$
\begin{aligned}
&\exp(\beta a\cos\theta')\{A_{s2}^{l}H_s^{(1)}(\kappa a)+B_{s2}^{l}H_s^{(1)}(\mathrm{i}\beta a)\}-C_{s2}^{l}J_s(\mathrm{i}\beta a)\\
&=-\exp[\beta(2h_1-a\cos\theta')]\\
&\times\Bigg\{A_{s1}^{l-1}\sum_{m=-\infty}^{\infty}H_{s-m}^{(1)}(2\kappa h_1)J_s(\kappa a)+B_{s1}^{l-1}\sum_{m=-\infty}^{\infty}H_{s-m}^{(1)}(2\mathrm{i}\beta h_1)J_s(\mathrm{i}\beta a)\Bigg\},\\
&\quad(l=2,3,\ldots,\infty).
\end{aligned}\tag{51}
$$

Eqs. (40)–(51) are the algebra equations determining the mode coefficients A_{n1}^{l}, A_{n2}^{l}, B_{n1}^{l}, B_{n2}^{l}, C_{n1}^{l} and C_{n2}^{l} of the scattered and refracted waves.

According to the definition of the dynamic stress concentration factor (DSCF), the DSCF is the ratio of the hoop shear stress around the cavity and the maximum stress result in from the incident waves (Pao and Mow, 1973). Thus, the DSCF around the circular cavity in FGPMs is expressed as

$$\mathrm{DSCF} = \tau^*_{\theta z} = |\tau_{\theta z}/\tau_0|. \tag{52}$$

Here,

$$\tau_{\theta z} = \frac{1}{r}\left\{c_{44}\frac{\partial u_z^t}{\partial \theta} + e_{15}\frac{\partial \phi^t}{\partial \theta}\right\}. \tag{53}$$

It should be noted that $\tau_0 = u_0\mu^e k$ denotes the maximum stress resulting from the incident waves.

Thus, the DSCF around the circular cavity in FGPMs is expressed as

$$\begin{aligned}
\mathrm{DSCF} &= \frac{e^{2\beta a\cos\theta}}{ka}\left\{\frac{\partial(u_z^i + u_{z1}^{(s)} + u_{z2}^{(s)})}{\partial\theta} - c_{44}^0\frac{\partial\psi_1^{(i)}}{\partial\theta} - c_{44}^0\frac{\partial\psi_1^{(s)}}{\partial\theta} - c_{44}^0\frac{\partial\psi_2^{(s)}}{\partial\theta}\right\} \\
&= \frac{e^{\beta a\cos\theta + h_1(i\kappa-\beta)}}{ka}\left\{\left[\beta a\sin\theta\sum_{n=-\infty}^{\infty} i^n J_n(\kappa a)e^{in\theta} + \sum_{n=-\infty}^{\infty} i^{n+1} n J_n(\kappa a)e^{in\theta}\right]\right. \\
&\quad \left.+\left[\beta a\sin\theta\sum_{l=1}^{\infty}\sum_{n=-\infty}^{\infty} A_{n1}^l H_n^{(1)}(\kappa a)e^{in\theta} + \sum_{l=1}^{\infty}\sum_{n=-\infty}^{\infty} inA_{n1}^l H_n^{(1)}(\kappa a)e^{in\theta}\right]\right\} \\
&\quad + \frac{e^{\beta(2b+3a\cos\theta)}}{ka}\left\{-\beta a\sin\theta\sum_{l=1}^{\infty}\sum_{n=-\infty}^{\infty}\sum_{m=-\infty}^{\infty}(-1)^{m-n}A_{n2}^l H_{m-n}^{(1)}(2\kappa b)J_m(\kappa a)e^{im\theta}\right. \\
&\quad \left.+\sum_{l=1}^{\infty}\sum_{n=-\infty}^{\infty}\sum_{m=-\infty}^{\infty}(-1)^{m-n} imA_{n2}^l H_{m-n}^{(1)}(2\kappa b)J_m(\kappa a)e^{im\theta}\right\} \\
&\quad - c_{44}^0\frac{e^{\beta a\cos\theta - 2\beta h_1}}{ka}\left\{\left[\beta a\sin\theta\sum_{n=-\infty}^{\infty} i^n J_n(i\beta a)e^{in\theta} + \sum_{n=-\infty}^{\infty} i^{n+1} n J_n(i\beta a)e^{in\theta}\right]\right. \\
&\quad \left.+\left[\beta a\sin\theta\sum_{l=1}^{\infty}\sum_{n=-\infty}^{\infty} B_{n1}^l H_n^{(1)}(i\beta a)e^{in\theta} + \sum_{l=1}^{\infty}\sum_{n=-\infty}^{\infty} inB_{n1}^l H_n^{(1)}(i\beta a)e^{in\theta}\right]\right\} \\
&\quad - c_{44}^0\frac{e^{\beta(2b+3a\cos\theta)}}{ka}\left\{-\beta a\sin\theta\sum_{l=1}^{\infty}\sum_{n=-\infty}^{\infty}\sum_{m=-\infty}^{\infty}(-1)^{m-n}B_{n2}^l H_{m-n}^{(1)}(2i\beta b)J_m(i\beta a)e^{im\theta}\right. \\
&\quad \left.+\sum_{l=1}^{\infty}\sum_{n=-\infty}^{\infty}\sum_{m=-\infty}^{\infty}(-1)^{m-n} imB_{n2}^l H_{m-n}^{(1)}(2i\beta b)J_m(i\beta a)e^{im\theta}\right\}.
\end{aligned} \tag{54}$$

6. Numerical examples and discussion

Fatigue failures often occur in regions with high stress concentrations, so an understanding of the distribution of the dynamic stress is very useful in structural design. According to the expression of DSCF, the DSCFs around the circular cavity are computed. It is found that the truncations after $l = 10$ and $n = m = 12$ give practically adequate results at any desired frequency. It is noted that the truncations of l, n and m are only related to the incident wave frequency, and the smaller truncated numbers of them can be adopted when the wave frequency is smaller.

In the following analysis, it is convenient to make the variables dimensionless. To accomplish this step, we may introduce a characteristic length a, where a is the radius of the cavity. The following dimensionless variables and quantities have been chosen for computation: the incident wave number is $ka = 0.1$–3.0, the position of the cavity beneath the surface of FGPM structure is $h_1/a = 1.1$–5.0 and $h_2/a = 1.1$–5.0, and the ratio of the material properties of the FGPMs is $p = c_{44}^2/c_{44}^1 = 0.2$—$5.0$.

To validate the present dynamical model, comparison with the previous literatures is given. Fig. 2 illustrates the angular distribution of the dynamic stress around the circular cavity with $p = 1.0$, $e_{15} = \varepsilon_{11} = 0$ and $h_1/a = 5.0$. $p = 1.0$ means that the functionally graded materials reduce to the homogeneous materials. $e_{15} = \varepsilon_{11} = 0$ implies that the piezoelectric effect is not taken into consideration. When the distance ratio is $h_1/a = 5.0$, the effect of the edge of the structure can be ignored. It can be seen that the angular distribution of DSCFs is symmetric about both axes when the dimensionless wave number is small. So, the effect of the boundary disappears. When $ka = 0.5$, the maximum value of DSCFs is about 2.0, and appears at the positions of $\theta = \pi/2, 3\pi/2$. Through comparison, it is found that the results coincide with those in an infinite homogeneous material (Datta et al., 1984; Fang et al., 2007; Rice and Sadd, 1984).

Fig. 3 illustrates the angular distribution of the DSCFs around the circular cavity with $p = 1.0$, $e_{15} = \varepsilon_{11} = 0$ and $h_1/a = 1.1$. It can be seen that when the buried depth is $h_1/a = 1.1$, because of the multiple scattering between the cavity and the edge of layer, the DSCFs at the illuminated sides of the cavity are greater than those at the shadow sides of the cavity. At the positions

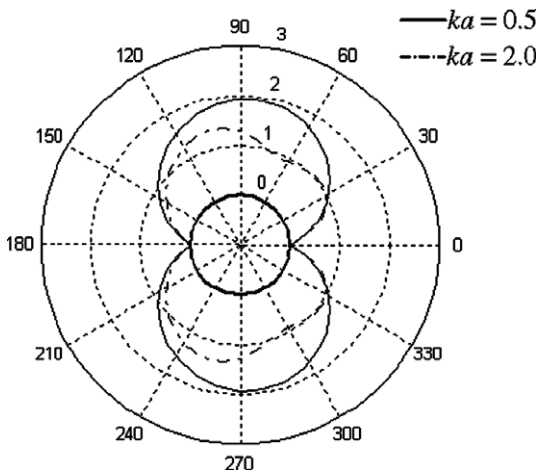

Fig. 2. Angular distribution of dynamic stress concentration factor around the cavity in an infinite homogeneous material without piezoelectric effects ($p = 1.0$, $e_{15} = \varepsilon_{11} = 0$, $h_1/a = 5.0$).

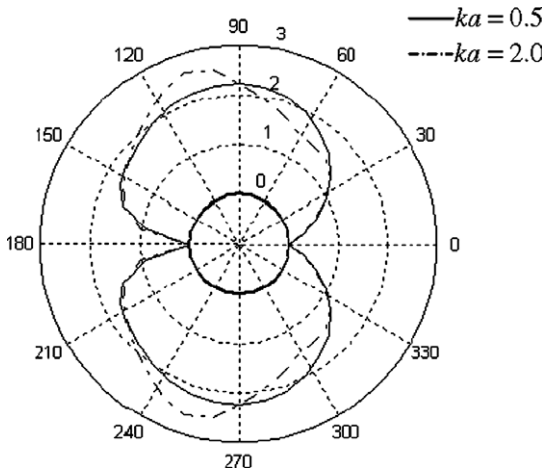

Fig. 3. Angular distribution of dynamic stress concentration factor around the cavity in a semi-infinite homogeneous material without piezoelectric effects ($p = 1.0$, $e_{15} = \varepsilon_{11} = 0$, $h_1/a = 1.1$).

of $\theta = 0, \pi$, the DSCFs are the minimum. Comparing the results in Figs. 2 and 3, it is clear that the effect of the edge of the structure on the dynamic stress in the region of high frequencies is greater than that in the region of low frequency.

Fig. 4 illustrates the angular distribution of the DSCFs around the circular cavity in a homogeneous piezoelectric material with $p = 1.0$ and $h_1/a = 1.1$. Comparing the results in Figs. 3 and 4, it is clear that the effect of the piezoelectric property on the dynamic stress in the region of high frequency is greater than that in the region of low frequency. At the illuminated sides of the cavity, the effect of the piezoelectric property on the dynamic stress is greater.

Figs. 5–7 display the angular distribution of the DSCFs around the circular cavity with $p = 2.0$ when the values of h_1/a and h_2/a are different. From Figs. 3–5, it can be seen that when the buried depth of the cavity and the thickness of the functionally graded layer are small, the dynamic stress near the boundary increases greatly. The greater the dimensionless wave number, the greater the increase of the dynamic stress near the boundary is. The maximum dynamic stress has a trend of shifting towards the illuminated side of the cavity. When the value of h_2/a becomes great, the boundary effect decreases. However, the effect of the value of h_1/a is much greater that of the value of h_1/a. Comparing the results in Figs. 5 and 6, it is clear that the increase of the value of h_2/a leads to the decrease of the dynamic stress near the boundary. In Figs. 5 and 7, it can be seen that when the buried depth of the cavity is relatively great, the thickness of the layer expresses little effect on the dynamic stress around the cavity.

Figs. 8–10 display the angular distribution of the DSCFs around the circular cavity with $p = 0.5$ when the values of h_1/a and h_2/a are different. From Figs. 2, 8 and 9, it can be seen that when the values of h_1/a and h_2/a are small, the distribution of the maximum dynamic stress has a trend of shifting towards the shadow side of the cavity, and the greater the dimensionless

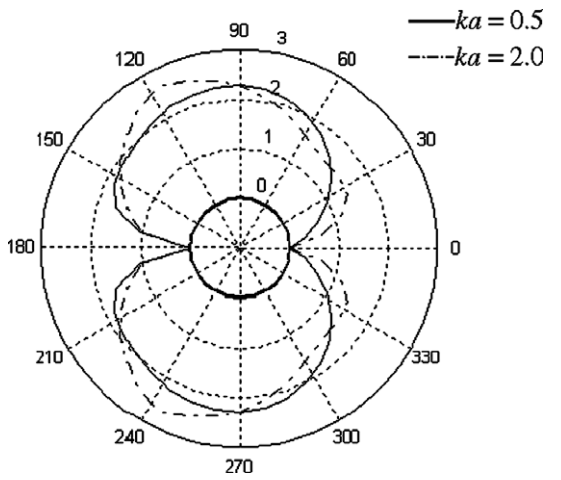

Fig. 4. Angular distribution of dynamic stress concentration factor around the cavity in a homogeneous piezoelectric material ($p = 1.0$, $h_1/a = 1.1$).

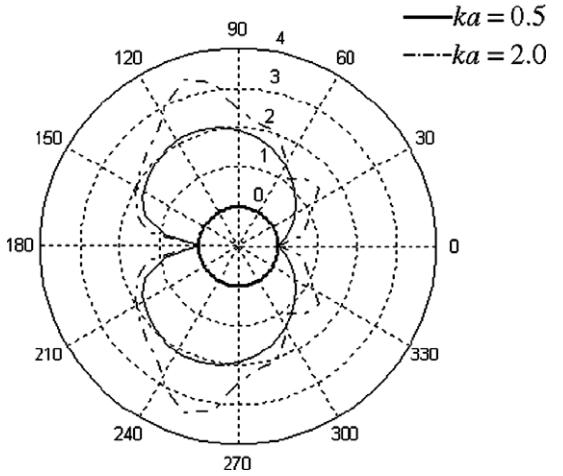

Fig. 5. Angular distribution of dynamic stress concentration factor around the cavity in the FGPM layer ($p = 2.0$, $h_1/a = 1.1$, $h_2/a = 1.1$).

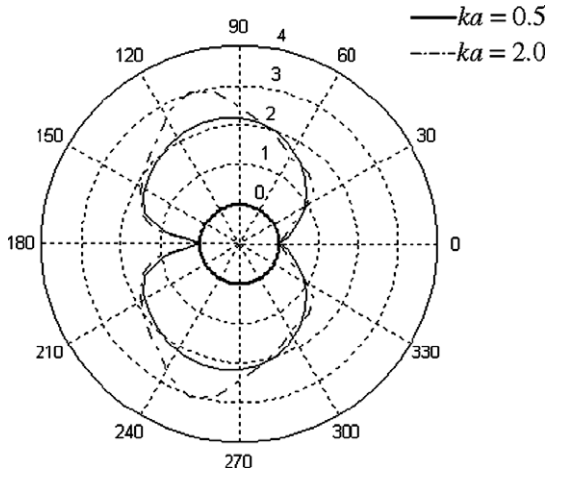

Fig. 6. Angular distribution of dynamic stress concentration factor around the cavity ($p = 2.0$, $h_1/a = 1.1$, $h_2/a = 5.0$).

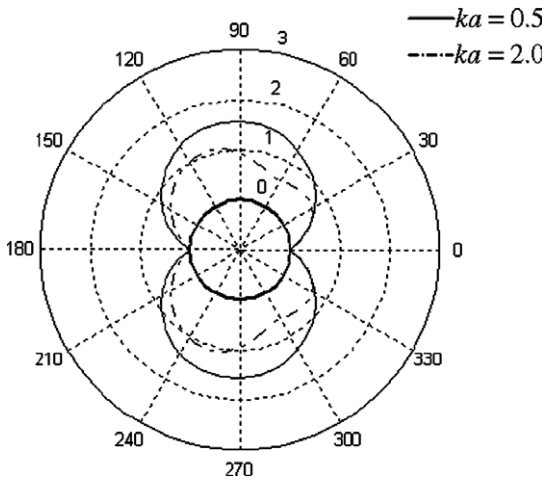

Fig. 7. Angular distribution of dynamic stress concentration factor around the cavity ($p = 2.0$, $h_1/a = 5.0$, $h_2/a = 1.1$).

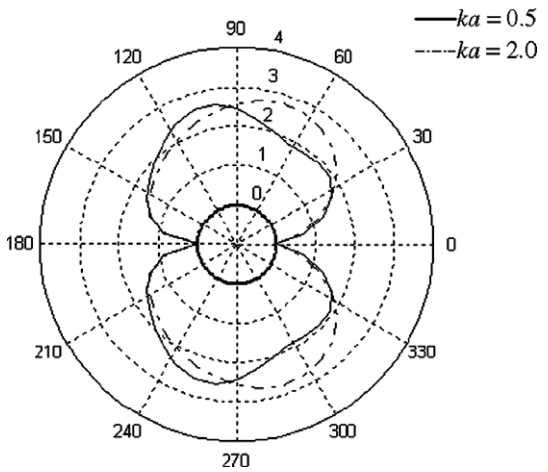

Fig. 8. Angular distribution of dynamic stress concentration factor around the cavity ($p = 0.5$, $h_1/a = 1.1$, $h_2/a = 1.1$).

wave number, the more distinct the shifting trend is. When the value of p is $p < 1.0$, the variation of the value of h_2/a only expresses effect on the dynamic stress at the shadow side of the cavity.

From Figs. 5–10, it is clear that the maximum dynamic stress around the cavity increases with the increase of the value of p. The effects of h_1/a and h_2/a on the dynamic stress around the cavity also increase with the increase of the value of p.

Fig. 11 shows the effect of the value of p on DSCFs at the position of $\theta = \pi/2$ as a function of the dimensionless wave number ka with parameters: $h_1/a = 1.1$ and $h_2/a = 1.1$. It can be seen that if the ratio $p < 1.0$, the variation of the DSCFs with dimensionless wave number is little, and the effect of the value of p on the dynamic stress is also little. However, when the ratio $p > 1.0$, the fluctuation of the DSCFs is great as the dimensionless wave number varies, and the greater the value of p, the more evident the fluctuation is. In the region of low frequency, the dynamic stress decreases with the increase of the value of p. In the region of higher frequencies, the dynamic stress increases with the increase of the value of p. The effect of wave frequency on the dynamic stress is greater when the ratio $p > 1.0$. The piezoelectric property in FGPMs makes the dynamic stress around the cavity become greater. The effect of the piezoelectric property on the dynamic stress is greater in the case of $p > 1.0$ than that in the case of $p < 1.0$. That is to say, when the material properties of the homogeneous piezoelectric material are greater than those at the surface of the structure, the dynamic stress resulting from the piezoelectric property is greater.

Fig. 12 shows the effect of the value of p on DSCFs at the position of $\theta = \pi/2$ as a function of the dimensionless wave number ka with parameters: $h_1/a = 1.1$ and $h_2/a = 5.0$. Comparing with the results in Fig. 11, it is found that with the increase of the thickness of FGPM layer, the effect of the value of p on the dynamic stress decreases greatly, especially when the value of p is $p > 1.0$. The effect of the piezoelectric property on the dynamic stress decreases with the increase of the thickness of the FGPM layer.

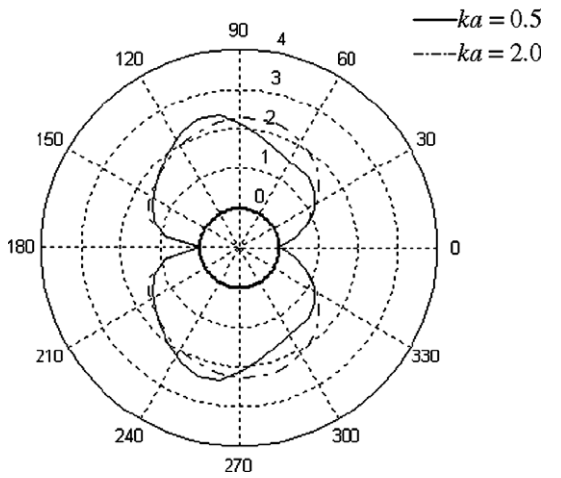

Fig. 9. Angular distribution of dynamic stress concentration factor around the cavity ($p = 0.5$, $h_1/a = 1.1$, $h_2/a = 5.0$).

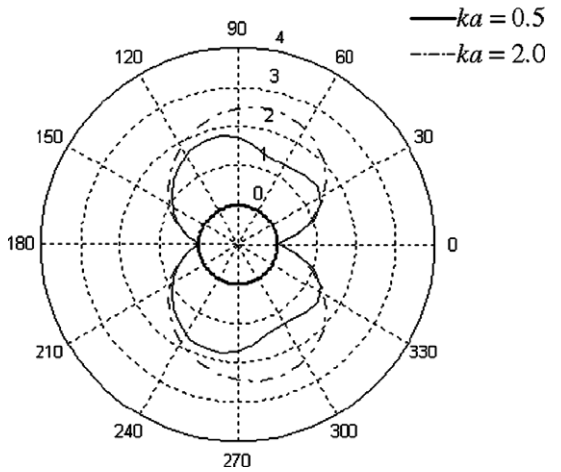

Fig. 10. Angular distribution of dynamic stress concentration factor around the cavity ($p = 0.5$, $h_1/a = 5.0$, $h_2/a = 1.1$).

7. Conclusions

The propagation and multiple scattering of electro-elastic waves in a functionally graded piezoelectric material layer with a circular cavity are investigated theoretically by employing image method and wave functions expansion method. The analytical solution and numerical solution of this problem are presented. For the homogeneous materials, our results are in good agreement with the solutions in previous literatures. Comparing with the solution in the static case, analysis shows that the piezoelectric property has great effect on the dynamic stress in the region of higher frequencies.

In contrast to the homogeneous medium, it is found that the graded property and piezoelectric property of FGPMs have great influence on the value and distribution of the dynamic stress concentration factors around the cavity. When the buried depth of the cavity and the thickness of the functionally graded layer are both small, the dynamic stress near the edge of the structure increases greatly. The greater the dimensionless wave number, the greater the increase of the dynamic stress around the cavity is. When the buried depth of the cavity is relatively great, the thickness of the layer expresses little effect on the dynamic stress around the cavity. The maximum dynamic stress around the cavity increases with the increase of the value of p. When the material properties of the homogeneous piezoelectric material are greater than those at the surface of the structure, the dynamic stress resulting from the piezoelectric property is greater.

Therefore, to reduce the dynamic stress and avoid fatigue failures of structures, it is proposed that the material properties of the homogeneous piezoelectric material are less than those at the surface of the structure. If the buried depth of cavity is smaller, a small value of p should be chosen. When the value of p is small, the thinkness of FGPM layer may be great. When designing the FGPMs under higher frequencies, the buried depth of cavity should be greater.

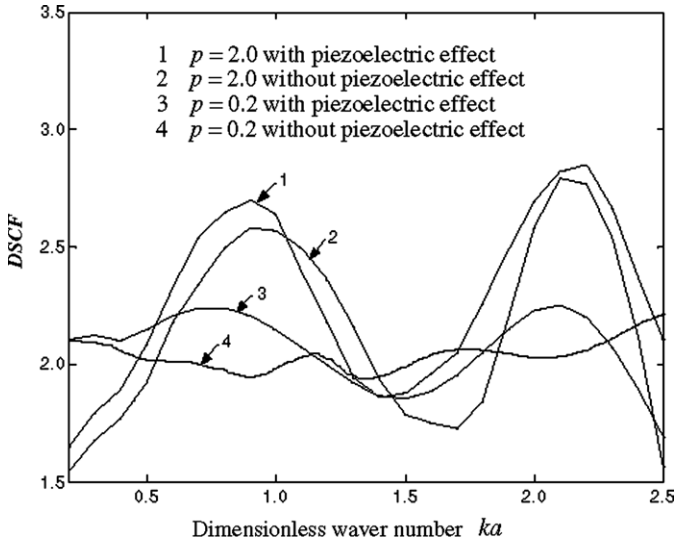

Fig. 11. Effect of material properties of FGM layer on dynamic stress concentration factor with $\theta = \pi/2$, $h_1/a = 1.1$, $h_2/a = 1.1$.

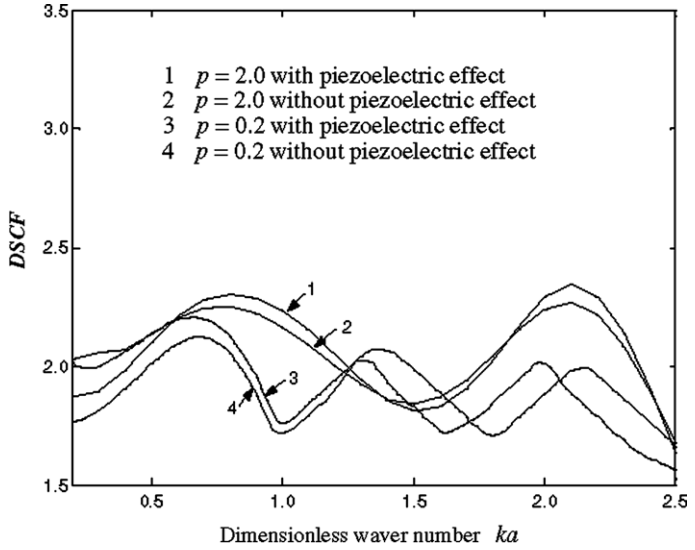

Fig. 12. Effect of material properties of FGM layer on dynamic stress concentration factor with $\theta = \pi/2$, $h_1/a = 1.1$, $h_2/a = 5.0$.

References

Chen, J., Liu, Z.X., Zou, Z.Z., 2003. Electromechanical impact of a crack in a functionally graded piezoelectric medium. Theoretical and Applied Fracture Mechanics 39, 47–60.

Chue, C.-H., Ou, Y.-L., 2005. Mode III crack problems for two bonded functionally graded piezoelectric materials. International Journal of Solids and Structures 42, 3321–3337.

Datta, S.K., Wong, K.C., Shan, A.H., 1984. Dynamic stresses and displacements around cylindrical cavities of arbitrary shape. ASME Journal of Applied Mechanics 51, 798–803.

Fang, X.Q., Hu, C., Du, S.Y., 2006. Strain energy density of a circular cavity buried in a semi-infinite functionally graded materials subjected to shear waves. Theoretical and Applied Fracture Mechanics 46, 166–174.

Fang, X.-Q., Hu, C., Huang, W.-H., 2007. Dynamic stress of a circular cavity buried in a semi-infinite functionally graded piezoelectric material subjected to shear waves. European Journal of Mechanics A 26, 1016–1028.

Li, C., Weng, G.J., 2002. Antiplane crack problem in functionally graded piezoelectric materials. ASME Journal of Applied Mechanics 69, 481–488.

Ma, L., Wu, L.-Z., Zhou, Z.-G., Guo, L.-C., Shi, L.-P., 2004. Scattering of harmonic anti-plane shear waves by two collinear cracks in functionally graded piezoelectric materials. European Journal of Mechanics A 23, 633–643.

Pao, Y.-H., Mow, C.C., 1973. Diffraction of Elastic Waves and Dynamic Stress Concentrations, Crane, Russak, New York.

Rice, J.M., Sadd, M.H., 1984. Propagation and scattering of SH-waves in semi-infinite domains using a time-dependent boundary element method. ASME Journal of Applied Mechanics 51, 641–645.

Soh, A.K., Fang, D.-N., Lee, K.L., 2000. Analysis of a bi-piezoelectric ceramic layer with an interfacial crack subjected to anti-plane shear and in-plane electric loading. European Journal of Mechanics A 19, 961–977.
Stratton, J.A., 1941. Electromagnetic Theory. McGraw-Hill, New York.
Wang, B.L., Noda, N., 2001. Thermal induced fracture of a smart functionally graded composite structure. Theoretical and Applied Fracture Mechanics 35, 93–109.
Wang, B.L., 2003. A mode III crack in functionally graded piezoelectric materials. Mechanics Research Communication 30, 151–159.
Zhou, Z.-G., Wu, L.-Z., 2006. Non-local theory solution for the anti-plane shear of two collinear permeable cracks in functionally graded piezoelectric materials. International Journal of Engineering Science 44, 1366–1379.